

## **ELECTRONIC SUPPLEMENTARY INFORMATION**

### **(a) ANATOMY**

Very few teeth of DORCM G 13,675 were found. The remains were sufficient to show that, in this specimen, as in most large Kimmeridgian forms, teeth were trihedral. As a consequence, a great deal of functional similarity can be assumed with *Pliosaurus westburiensis* and *Pliosaurus carpenteri* (BRSMG Cc332 and BRSMG Cd6172) (Sassoon *pers comm*).

### **(b) MUSCLE RECONSTRUCTION**

Once the insertion areas were identified, 3D muscle reconstruction was carried out following procedures described in Lautenschlager (2013). Rods linking the insertion and origin surfaces were produced in order to evaluate the intersection between various muscle groups and provide an estimated idea of the volume occupied by each. Muscle masses were then fleshed out along the lines of action, until muscle volumes occupied the whole temporal fossa. Overlaps were solved following the geometric relations described in the literature (Romer, 1956; Cleuren & De Vree, 2000; Holliday & Witmer, 2007; Holliday, 2009, Bates & Falkingham, 2012). Muscle reconstruction and lever calculations have been used to produce and compare anatomical information and bite force for many extant and extinct taxa such as crocodylians, mammals, dinosaurs and in general for archosaurs (Thomason, 1991; Cleuren & De Vree, 2000; Holliday & Witmer, 2007; Holliday, 2009).

The pliosaur adductor muscles were grouped as the *M. adductor mandibulae externus* (*M. ame*), *M. adductor mandibulae posterior* (*M. amp*), *M. pseudotemporalis* (*M. pst*), and *M. pterygoideus* (*M. pt*). In the last of these, it was not possible to distinguish the pars dorsalis and pars ventralis owing to poor preservation of the attachment areas of the former. For this reason, the two masses were modelled as a unique group combined despite the evidence in modern reptile and birds that they have different insertion areas; this operation took account of the volume supposedly occupied by *M. ptd* and merged it with *M. ptv*; the latter is laterally unconstrained by the mandible

bones and it acts as a first-order pulley, which makes it difficult to model; however the discrimination of the two groups is to a certain extent arbitrary and they are often modelled as a single mass (Taylor, 1992; Taylor & Cruickshank, 1993; Cleuren & De Vree, 2000; Holliday & Witmer, 2007; Holliday, 2009).

### (c) BEAM THEORY

Elongate snouts are common in extant and extinct aquatic predators. In this respect, crocodilians, crown cetaceans, ambulocetes and to a certain extent the terrestrial spinosaurid dinosaurs represent cases of morphological convergence with pliosaurs. The advantages in considering crocodiles as the best comparative taxa to pliosaurs are multiple, in particular crocodilians and pliosaurs share the feature of an akinetic skull.

BoneJ (Doubé et al. 2010) standard “Geometry slice” analysis returns maximum and minimum moment of areas  $I_{min}$  and  $I_{max}$ . However, if the structure analysed varies in section shape, or its maximum and minimum axes do not coincide with dorso-ventral and lateral directions, the results lose their significance. For the snout, this problem is not important because  $I_x \equiv I_{min}$  and  $I_y \equiv I_{max}$  for all the taxa except *Baryonyx* in which the opposite situation occurs. Here, Y, is the medio-lateral axis and X is the dorso-ventral axis. The second moment of area scales to  $Area^2$ , then to  $length^4$ :  $I = \sum d^2 \Delta A$  where  $d$  = distance from neutral axis;  $\Delta A$  = area of a strip of material.

#### *Crocodylian ecomorphological space*

McHenry *et al.* (2006) proposed four ecomorphological types for crocodilians; (a) longirostrine, (b) brevirostrine; and (c) mesorostrine, subdivided into two sub-groups: (i) taller and narrower; (ii) broader and flatter. Not surprisingly, exceptions and overlaps in these classes are common and they are accounted for both by different ontogenetic stages (Cleuren & De Vree, 2000) and dimensions.

(a) Longirostrine. Includes forms such as *Gavialis gangeticus*, *Mecistops cataphractus*. Their

rostra are elongated, and laterally and dorsoventrally compressed. On the one hand, their snout allows faster and more precise subaqueous lateral sweeps, but on the other, they are mechanically weak because of the length and the small CSA. Not by chance are they mainly specialist piscivores (McHenry et al. 2006). Narrow rostra also minimize the force required to expel water from the mouth when the jaws close on a prey item (Seymour, 1982).

**(b) Brevirostrine.** Includes *Osteolaemus* and a few other living short-snouted taxa. Their diet is represented by small terrestrial animals and underwater invertebrates rather than small and agile fish (McHenry et al. 2006).

**(c) Mesorostrine.** Most living crocodilians and the larger forms fall in this group. Fish represent a prominent part of their diet and the skull depths are reduced. Their rostra have modest depth and are considerably broader; this latter feature increases the moments of area and so bending and torsional resistance. Together with the reduction of rostrum length (shorter snouts means shorter out-lever arms) and large dimensions (see next paragraph), this allows mesorostrines to adopt a generalized diet, which sometimes includes middle-sized and large mammals. The two subgroups represent a simplification of the continuous variation from a relatively higher and narrower snout (i), such as *Crocodylus niloticus*, to a broader and flatter snout (ii), such as *Alligator mississippiensis* and *Caiman crocodylus*.

In addition we call broad-snouted crocodiles 'latirostrine', following Mueller-Töwe (2006), regardless of the length of the snout. In our analyses, McHenry's subdivision is broadly followed; *Gavialis gangeticus* falls in (a) and its standardised resistances are lower than *Crocodylus niloticus* (c-i), and then *Alligator mississippiensis* and *Caiman crocodylus* both in (c-ii). In this regard, our study confirms this, which is thoroughly explained by Cuff and Rayfield (2013).

#### **(d) BITE FORCE**

Muscle force can be calculated knowing the maximum cross sectional area (MCSA), calculated on a plan perpendicular to the line of action, and the average tension of muscle material  $t$  with the

79 formula:  $F = CSA * t$

80  $t$  was assumed equal of 30 N/cm<sup>2</sup> as adopted in many other studies (Thomason, 1991; Wroe et al.  
81 2005; Wroe et al. 2007a; Wroe et al. 2007b; Lautenschlager, 2013). It is noteworthy that this value  
82 is debated and there are studies showing that reptilian estimates may be even higher, up to 89 N/cm<sup>2</sup>  
83 for *Sphenodon* (Curtis et al. 2010).

84 Along with the application of classic lever mechanics for calculating bilateral and unilateral  
85 bite forces, this study also adopted a method which takes account of both muscle masses for  
86 unilateral bites (Fig. S1). Lower jaws can be represented by a type III lever where the fulcrum is  
87 represented by the articular surfaces ( $Jr$  and  $Jl$ ), the effort by the muscle forces ( $Fr$ ,  $Fl$ ) and the  
88 resistance is placed at the bite position (B1-5).

89 The traditional 2D lever model collapses all forces to the sagittal plane or along the  
90 mandibular ramus. In particular, unilateral bite geometry relies on the assumption that the input  
91 force ( $Fi$ ) is the force exerted by both muscle masses (which is not always geometrically possible).  
92 These values are simply distributed on two symmetric biting positions in the bilateral setting.

93 Greaves (1983) showed that for carnivores, unilateral bite positions are better represented by  
94 a slightly different system which takes account of the inputs from both sides and recreates a  
95 simplified triangular geometry in which the functional lever is not on the sagittal plane but runs  
96 from the bite point to J, the functional joint on the joint line ( $Jl-Jr$ ), passing thorough  $F$ , the location  
97 where muscle resultant force is applied (Fig. S1B). The mechanical advantage does not change with  
98 respect to the traditional method. However, forces need to be vertically oriented; for this reason,  
99 vertical components of each muscle group were calculated. We applied these concepts to the lower  
100 jaw of the pliosaur which, despite a different geometry, can be considered subject to the same  
101 principles.

102 Comparisons made with other models, particularly crocodiles and *Kronosaurus*  
103 *queenslandicus* (McHenry, 2009), suggest that *M. pt* volume might have been underestimated  
104 relative to the other muscular masses. For this reason, bite force estimations were reported in two

versions; the original one and a corrected version assuming a *M. pt* CSA roughly equal to half of the total CSA calculated for the sum of *M. ame*, *M. amp*, *M. pst* as data from McHenry (2009) suggest for *Kronosaurus queenslandicus* and *Crocodylus porosus*.

#### (e) FEA

The effect of the mandibular symphyseal suture on the analysis and distribution of stresses was evaluated by modelling a suture on the sagittal plan of the mandibular symphysis. When adding a symphyseal suture, rostral stress spreads on to the ventrolateral surface of the mandibular symphysis.

*Lower jaw.* In the unilateral bite models, von Mises and principal strain patterns indicate that the balancing side bends dorsally between the jaw joint and mandibular symphysis. The unilateral FE models (Fig S2F-J, S4) return a picture that is comparable to what was described for an analogous study on the mandible of *Alligator mississippiensis* (Porro et al. 2011). In both unilateral and bilateral bites, the structure incurs higher stress where the bite is exerted by the symphyseal teeth, B4 and B5 in figure S2-3. The pull of both muscles (bF), acting at the same time on both mandibular rami, amplifies stress on the weak areas of the jaws when bite constraints are placed on the mandibular symphyses.

With the rostral shift of the bite positions (B4, B5), the reaction on the balancing side (Fig. S3A) does not change; the amount of stress only increases. On the whole, the balancing ramus always bends dorsally with a torsional component.

On the working side the situation is more complicated (Fig. S3B). The forces acting on it are the muscle pull of the working side (F) and the muscle pull from the balancing (bF) side which is transmitted along the ramus and applied at the symphysis; in the middle there is a restrained bite position (Fig. S3). Bite locations posterior to the mandibular symphysis (such as B1, B2 in Figure S2), oppose the pulling force of the muscle, so creating a compressive area along the tooth row; a low stressed area is between B1/B2 and F represents an inflection point (I) (Fig. S3B) where the

131 ramus bending orientation changes. Posteriorly, the tension is dorsal, anteriorly it is ventral and vice  
 132 versa. The size of the areas changes with the location of the bite constraint.

133         Conversely, when the bite position occurs at the mandibular symphyses (B4, B5,), bF and F  
 134 can act symmetrically on both the rami, creating a situation in which their dorsal sides are under  
 135 tension and their ventral sides are compressed (Fig. S2D-E, I-J). In these cases, most stress is  
 136 concentrated in the narrow area caudal to the mandibular symphysis, which has to deal with the  
 137 force input of both muscular masses without attenuation of constraints in the middle of the jaw.

138         A certain rotational component occurs on both working and balancing side. It acts on the  
 139 whole ramus but it is particularly evident on the dorsal edge of high area across the coronoid  
 140 process which is bent towards the sagittal plane.

141         The von Mises representations of the posterior bilateral models show that stress does not  
 142 propagate rostrally to the bite positions (bF is 'stopped' along each ramus at B1 and B2). However,  
 143 when rostral bite positions are constrained, the caudal end of the symphysis shows again high stress  
 144 because bF acts on both ramii caudally of the constraints. Thus in this case the same considerations  
 145 reported for the working side of the unilateral model explain also the bilateral models.

146 At caudal loads, a lower amount of stress is generated in the weakest area.

- 147         1. Moving the loads caudally, the mechanical advantage increased because of reduction of the  
 148 out-lever arm length, and this allowed higher forces to be applied than are possible with a  
 149 longer lever.
- 150         2. The largest alveoli, for the 3<sup>rd</sup>-4<sup>th</sup>-5<sup>th</sup> premaxillary teeth and the corresponding teeth on the  
 151 dentary are sited in line across this area. The most robust teeth are deeply rooted in the  
 152 premaxillae and anterior maxillae in many genera, including *Pliosaurus*, *Liopleurodon* and  
 153 *Kronosaurus* (Noè 2001; McHenry 2009; Sassoon et al. 2012). Tooth size, proportions and  
 154 wear of the crown are linked with the forces and the mechanical properties of the prey items  
 155 they have to deal with (Massare 1987; Martill et al. 1994). Teeth are slightly curved, with a  
 156 low height-diameter ratio (2.0-3.0), similar to modern killer whales. Comparison suggests

that large bony prey items (such as fish and other reptiles) were part of the pliosaur diet. The triangular wear-carrying sharp ridges, typical of the largest reptiles in Jurassic faunas, also suggests that processing was common (Massare 1987; Martill et al. 1994).

Also in the lower jaws, suture morphology matches the predicted tensional regime in the dorsal half of the beam. The splenial, dentary and coronoid contacts are resolved as flat or overlapping sutures where the dorsal elements are overlapped by the more ventral ones. The coronoid overlaps the dentary, which touches the splenial through a butt-jointed contact. The splenial-coronoid contact is ambiguous and the CT scans do not fully resolve it. The suture geometry in this area is not surprisingly consistent with compressional and torsional regimes, considering the lower jaws would have been subjected to strong torsional and bending forces.

#### **(f) DIET**

In order to evaluate possible prey items of DORCM G.13,675, a table of length and body mass of the marine reptiles found in the Kimmeridgian of the UK was created (Figure S4). Plesiosaur body size and mass were calculated from pre-existing models (McHenry 2009). For thalattosuchian crocodiles, ichthyosaurs and turtles, regression lines describing length-mass relationships were calculated from the available literature on modern crocodiles, cetaceans and sea turtles (Table S3).

Given the similar size of their skulls (around 2m of length), it is a safe assumption that *Kronosaurus* and DORCM G.13,675 held the same place in their respective trophic webs. As a consequence, the largest gut contents of the Australian pliosaur provide a chance to evaluate the relative size of the prey items that DORCM G.13,675 could process and prey upon. This can be achieved by rescaling the dimensions (length and mass) of prey items and predators while maintaining the same dimensional ratios. In particular, the largest taxon found in the *Kronosaurus* gut content is a seized piece of torso belonging to a plesiosaur that was estimated to be, in life, roughly 40% the pliosaur's length and 3.4 % its weight; *Kronosaurus* bite marks on the skull of a larger plesiosaur (estimated to be 67% the length and 16% the weight of its predator) provide data

183 on the upper limit of the largest animal that could be preyed upon. By applying these limits to the  
184 Kimmeridgian taxa and to *Pliosaurus kevani*, we show the maximum dimensions of taxa that a  
185 pliosaur of the size of DORCM G.13,675 could capture and dismember.

186 A literature search was carried on in order to compile a database of all Kimmeridgian marine  
187 reptiles. Five groups were considered - Testudines, Thalattosuchia, Pliosaurioidea, Plesiosaurioidea  
188 and Ichthyosauria. When possible, each species was specified, although most of the dimension  
189 evaluations were produced at generic level. Only the taxa for which it was possible to find an  
190 estimate of dimensions were listed, hence it is not a complete formal list. Where possible a  
191 maximum and a minimum estimated size were given.

192 Total lengths were obtained from the literature. With regard to pliosaurs, lengths were  
193 obtained by applying the relationships between TL/SL (total length/skull length) as reported in  
194 McHenry's study. Skull lengths for pliosaurs were obtained from the literature and direct  
195 measurements on DORCM G.13,675.

196 Most of the data we adopted were summarised in Benton and Spencer (1995); for other taxa,  
197 we found dimensional estimates in the available literature: *Machimosaurus* (D. Naish, pers.  
198 comm.); *Plesiosuchus manselii* (Young et al. 2012); *Aegirosaurus* (Bardet & Fernández, 2000);  
199 *Plesiosaurus* sp. (Storrs, 1997); *Colymbosaurus trochanterius* (Owen 1840); *Kimmerosaurus*  
200 ([www.plesiosauria.com](http://www.plesiosauria.com)); *Thalassemys hugii* (Mlynarski, 1976).

201 In order to better estimate the volume for thalattosuchian, ichthyosaurs and testudines, these  
202 taxa were assumed to have the same TL/V ratio as crocodilians, middle-small cetaceans and modern  
203 sea turtles respectively; these were calculated in Openoffice 3.4 Calc after creating graphs of TL/V  
204 using entries from the literature. Thalattosuchians and fossil testudines are morphologically similar  
205 to extant crocodilians and turtles. On the contrary, ichthyosaurs are not close relatives of cetaceans,  
206 but they represent a case of morphological convergence, and possibly occupied similar ecological  
207 niches (Massare 1987; Martill et al. 1994). Length (L) scales to volume (V) following a cubic  
208 relationship; if the density of the body is assumed to be equal to the density of the water, then V can



209 be substitutes by Mass (M) in:

210 
$$(3) \quad V = aL^b$$

211 Various models that estimate V starting from body length TL already exist; McHenry (2009)  
212 used those produced by Invicta Plastics Ltd for the BMNH for pliosaurs and plesiosaurs. In this  
213 study, McHenry's data were plotted in an X-Y scatter graph using Openoffice 3.4 Calc; the  
214 regression line was calculated and its values (Table S3) were applied to the length for each pliosaur,  
215 for which the volume was not already calculated, in particular to DORCM G.13, 675. The same was  
216 done for plesiosaur estimated lengths.

217 Pliosaurids are the largest documented Kimmeridgian taxa. The pliosaur skull scales to body  
218 length at 1:4 to 1:5 (McHenry, 2009), indicating an estimated total body length for the Dorset  
219 pliosaur of 10.4 to 12.6 m.

220 The fossil record and our calculations suggest that large pliosaurs could prey on most taxa  
221 less than 16% of their body mass and 67% of their body length, which includes the vast majority of  
222 the Late Jurassic marine fauna. In fact, excluding a few exceptions such as *Pliosaurus*,  
223 *Machimosaurus*, *Ophthalmosaurus*, and *Plesiosuchus* (in their adult ontogenetic stages), all the taxa  
224 fall in the size range of prey that could be threatened by the largest Kimmeridgian pliosaurs (Fig. 3).  
225 However, there is evidence of actual feeding on prey items under 40% of the predator's total length.

227 **REFERENCES**

228

229 **Andrews CW** (1910) A descriptive catalogue of the marine reptiles of the Oxford Clay - based on  
 230 the Leeds collection in the British Museum (Natural History), London, Part I. British Museum  
 231 (Natural History), London, xxiii + 202 pp.

232 **Bardet N, Fernández M** (2000) A new ichthyosaur from the Upper Jurassic lithographic  
 233 limestones of Bavaria. *J Paleontol* **74**, 503-511.

234 **Benton MJ, Spencer PS (1995)** *Fossil reptiles of Great Britain*. Joint Nature Conservation  
 235 Committee, Geological Review Series, Volume 10. Chapman & Hall, London.

236 **Busbey AB** (1995) The structural consequences of skull flattening in crocodilians. In: Thomason,  
 237 J.J., editor. *Functional morphology in vertebrate paleontology*. Cambridge: Cambridge  
 238 University Press. p 173–192.

239 **Charig A, Milner A** (1986) *Baryonyx*, a remarkable new theropod dinosaur. *Nature* 324, 359-361.

240 **Clarke JB, Etches SM** (1992) Predation amongst Jurassic marine reptiles. *Proceedings of the*  
 241 *Dorset Natural History and Archaeological Society* **113**, 202-205.

242 **Cleuren J, De Vree F** (2000) Feeding in crocodilians. In *Feeding: form, function, and evolution in*  
 243 *tetrapod vertebrates*: 337–358. Schwenk, K. (Ed.). San Diego: Academic Press.

244 **Curtis N, Jones MEH, Lappin AK, et al.** (2010) Comparison between in vivo and theoretical bite  
 245 performance: Using multi-body modelling to predict muscle and bite forces in a reptile skull.  
 246 *Journal of Biomechanics* **43**, 2804-2809.

247 **Doube M, Klosowski M, Arganda-Carreras I, et al.** (2010) BoneJ Free and extensible bone  
 248 image analysis in ImageJ. *Bone* **47**, 1076-1079.

249 **Gómez-Pérez M** (2008) The palaeobiology of an exceptionally preserved Colombian pliosaur  
 250 (Sauropterygia: Plesiosauria). Unpublished PhD thesis, University of Cambridge, Cambridge,  
 251 xv + 243 pp.

252 **Greaves** (1983) A functional analysis of carnassial biting. *J Linn Soc* **20**, 353-363.

- Holliday C** (2009) New insights into dinosaur jaw muscle anatomy. *Anat Rec* **292**, 1246-1265.
- Holliday C, Witmer L** (2007) Archosaur adductor chamber evolution: Integration of musculoskeletal and topological criteria in jaw muscle homology. *J Morph* **268**, 457-484.
- Lautenschlager S** (2013) Cranial myology and bite force performance of *Erlikosaurus andrewsi*: a novel approach for digital muscle reconstructions. *J Anat* **222**, 260-272.
- Martill D, Taylor M, Duff K, et al.** (1994) The trophic structure of the biota of the Peterborough Member, Oxford Clay Formation (Jurassic), UK. *J Geol Soc* **151**, 173-194.
- Massare JA** (1987) Tooth morphology and prey preference of Mesozoic marine reptiles. *J Vert Paleontol* **7**, 121-137.
- McHenry CR** (2009) 'Devourer of Gods' - The palaeoecology of the Cretaceous pliosaur *Kronosaurus queenslandicus*. Unpublished PhD thesis, University of Newcastle, Newcastle, x + 616 pp.
- McHenry C, Clausen P, Daniel W, et al.** (2006) Biomechanics of the rostrum in crocodilians: A comparative analysis using finite-element modeling. *Anat Rec* **288A**, 827-849.
- McHenry C, Wroe S, Clausen P, et al.** (2007) Supermodeled sabercat, predatory behavior in *Smilodon fatalis* revealed by high-resolution 3D computer simulation. *Proc Natn Acad Sci, USA* **104**, 16010-16015.
- Mlynarski M** (1976). *Testudines*. Encyclopaedia of Paleoherpertology **7** i-vi, 1-130.
- Mueller-Töwe IJ** (2006) Anatomy, phylogeny, and palaeoecology of the basal thalattosuchians (Mesoeucrocodylia) from the Liassic of Central Europe. Unpublished PhD thesis, Universität Mainz, Germany. 422 pp.
- Noè LF** (2001) A taxonomic and functional study of the Callovian (Middle Jurassic) Pliosauroida (Reptilia, Sauropterygia). Unpublished PhD thesis, University of Derby, Derby, volume 1, xix + 347 pp; volume 2, xix + 182 pp.
- Patterson C** (1975) The braincase of pholidophorid and leptolepid fishes, with a review of the actinopterygian braincase. *Philos Trans R Soc Lond B* **269**, 282-283.

- 279 **Porro L, Holliday C, Anapol F, et al.** (2011) Free body analysis, beam mechanics, and finite  
280 element modeling of the mandible of *Alligator mississippiensis*. *J Morph* **272**, 910-937.
- 281 **Rayfield E** (2005) Aspects of comparative cranial mechanics in the theropod dinosaurs  
282 *Coelophysis*, *Allosaurus* and *Tyrannosaurus*. *J Linnean Soc* **144**, 309-316.
- 283 **Romer AS** (1956) *Osteology of the reptiles*. University of Chicago Press, Chicago, 772 pp.
- 284 **Sassoon J, Noè LF, Benton MJ** (2012) Cranial anatomy, taxonomic implications and  
285 palaeopathology of an Upper Jurassic Pliosaur (Reptilia: Sauropterygia) from Westbury,  
286 Wiltshire, UK. *Palaeontology* **55**, 743-773.
- 287 **Seymour KS** (1982). Physiological adaptations to aquatic life. In C. Gans & F. H. Pough (Eds).  
288 *Biology of the Reptilia* **13**, 1-51. London: Academic Press.
- 289 **Storrs GW** (1997) Morphological and taxonomic clarification of the genus *Plesiosaurus*. In:  
290 *Ancient Marine Reptiles* (eds J. M. Callaway, E. Nicholls), 145-190. New York: Academic  
291 Press.
- 292 **Tarlo LB** (1959) *Stretosaurus* gen. nov., a giant pliosaur from the Kimmeridge Clay.  
293 *Palaeontology* **2**, 39-55.
- 294 **Taylor MA** (1992) Functional anatomy of the head of the large aquatic predator *Rhomaleosaurus*  
295 *zetlandicus* (Plesiosauria, Reptilia) from the Toarcian (Lower Jurassic) of Yorkshire, England.  
296 *Proc R Soc Lond B* **335**, 247-280.
- 297 **Taylor MA, Cruickshank A** (1993) Cranial anatomy and functional morphology of *Pliosaurus*  
298 *brachyspondylus* (Reptilia, Plesiosauria) from the Upper Jurassic of Westbury, Wiltshire.  
299 *Philos Trans R Soc Lond B* **341**, 399-418.
- 300 **Taylor MA, Norman DB, Cruickshank ARI** (1993) Remains of an ornithischian dinosaur in a  
301 pliosaur from the Kimmeridgian of England. *Palaeontology* **36**, 357-360.
- 302 **Thomason JJ** (1991) Cranial strength in relation to estimated biting forces in some mammals. *Can*  
303 *J Zool* **69**, 2326-2333.
- 304 **Thomson KS** (1995) Graphical analysis of dermal skull roof patterns. In: *Functional Morphology*

- 305       in *Vertebrate Paleontology* (ed. J. J. Thomason), 193-204. Cambridge: Cambridge University  
306       Press.
- 307       **Wahl W** (1998) Plesiosaur gastric contents from the upper Redwater Shale (lower Oxfordian) of  
308       the Sundance Formation (Jurassic) of Wyoming. *J Vert Paleontol* 18, 84A.
- 309       **Wroe S, McHenry C, Thomason J** (2005) Bite club: comparative bite force in big biting  
310       mammals and the prediction of predatory behaviour in fossil taxa. *Proc R Soc B* **272**, 619–625
- 311       **Wroe S, Clausen P, McHenry C, et al.** (2007a). Computer simulation of feeding behaviour in the  
312       thylacine and dingo as a novel test for convergence and niche overlap. *Proc R Soc B* **274**, 2819-  
313       2828.
- 314       **Wroe S, Moreno K, Clausen P, et al.** (2007b). High-resolution three-dimensional computer  
315       simulation of hominid cranial mechanics. *Anat Rec* **290**, 1248-1255.
- 316       **Young MT, Brusatte SL, De Andrade MB, et al.** (2012) The cranial osteology and feeding  
317       ecology of the metriorhynchid crocodylomorph genera *Dakosaurus* and *Plesiosuchus* from the  
318       Late Jurassic of Europe. *PLoS ONE* **7**(9), e44985 (doi:10.1371/journal.pone.0044985).

319 **TABLE S1.** Detail of the CT scan material for each specimen.

Taxon	Specimen	Skull length [mm]	Scan Resolution		Slice Thickness [mm]	Field of reconstruction [mm]	Pixel size [mm]	CT scans	
								N° of scans used for beam theory	Tot
<i>Ostolaemus tetraspis</i>	FMNH 98936	96	1024x1024		0.11	56x56	0.0547	180	870
<i>Alligator mississippiensis</i> juvenile	TMM M-6723	54	1024x1024		0.08	38.6x38.6	0.0377	142	679
<i>Alligator mississippiensis</i> subadult	OUVC 9761	184	512x512		0.48	287x287	0.5600	97	384
<i>Crocodylus niloticus</i>	RNC AN1	630	512x512		3	400x400	0.7813	56	210
<i>Mecistops cataphractus</i>	BMNH 1924.5.10.1	685	512x512		5	280x280	0.5469	43	137
<i>Gavialis gangeticus</i>	BMNH 2005.1605	800	512x512		5	320x320	0.6250	52	161
<i>Caiman crocodilus</i>	FMNH 73711	132	1024x1024		0.14	67x67	0,0564	108	
<i>Baryonyx walkeri</i>	BMNH R9951	---	---		1.25	151x151 (pmx)	---	144	
						188x188 (mx)			
Weymouth bay pliosaur	DORCM G 13,675	2100	skull_01	512x512	1.5	269x269	0.5256	69	---
			skull_02	512x512	3	489x489	0.9546		---
			skull_03	512x512	3	489x489	0.9546	---	---
			skull_04	512x512	3	489x489	0.9546	---	---
			skull_05	512x512	3	554x554	1.0815	---	---
			skull_06	512x512	3	425x425	0.8300	---	---
			skull_07	512x512	3	425x425	0.8313	---	---
			skull_08	512x512	3	425x425	0.8313	---	---
			Jaw_01	512x512	3	259x259	0.5066	---	
			Jaw_02	512x512	3	259x259	0.5066	---	
			Jaw_03	512x512	3	489x489	0.9546	---	
			Jaw_04	512x512	3	489x489	0.9546	---	
			Jaw_05	512x512	3	489x489	0.9546	---	
			Jaw_06	512x512	3	489x489	0.9546	---	

321 **TABLE S2.** Geometrical details of adductor muscle groups.

<b>Muscle</b>	<b>Volume [cm<sup>3</sup>]</b>	<b>Origin- insertion distance [cm]</b>	<b>MCSA [cm<sup>2</sup>]</b>	<b>% musculature volume</b>	<b>Distance to hinge [cm]</b>
<i><b>M.ame</b></i>	22799.2	39.42	664.25	49	39.7
<i><b>M.amp</b></i>	5362.88	21.5	272.82	11	15.6
<i><b>M.pst</b></i>	8956.48	40.89	275.48	19	37.5
<i><b>M.pt</b></i>	9624.47	65.88	210.16	21	14.8

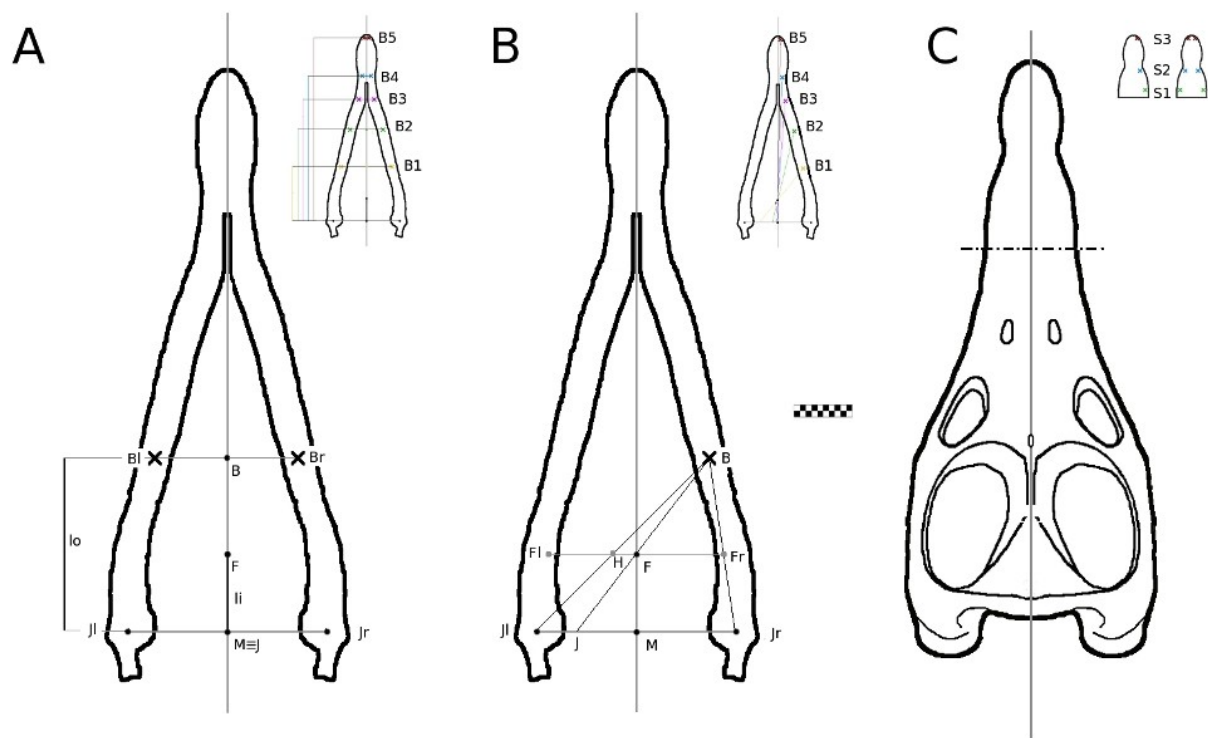
322

**Table S3.** Body length-volume(mass) relationships data. Parameters a, b refers to the equation  $V = aL^b$

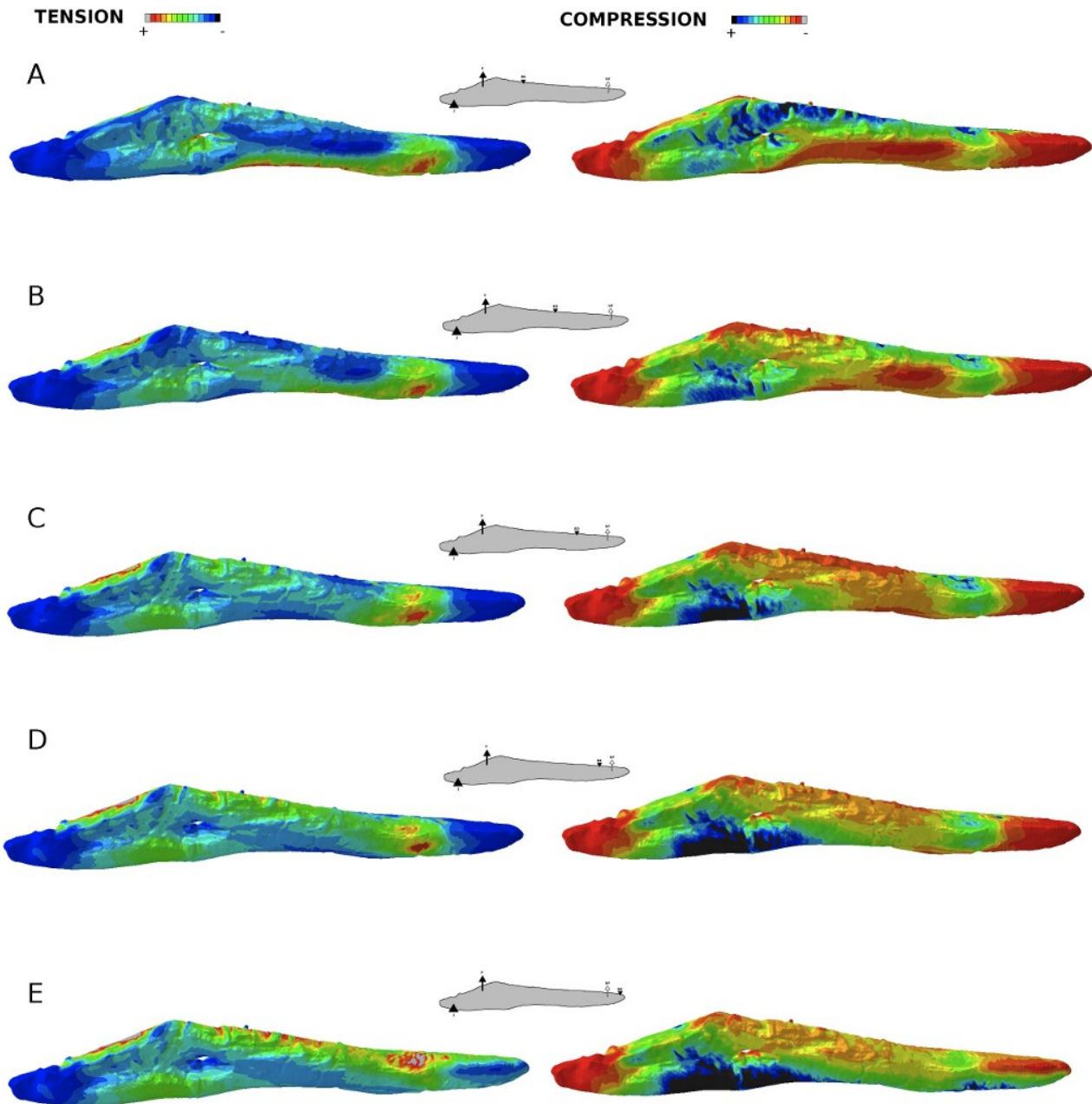
Group	Taxa adopted	a	b	R <sup>2</sup>	Sources
Crocodiles	<i>Alligator mississippiensis</i>	$9.7 \times 10^{-7}$	3.18	---	Hurlburt 1999
Cetaceans	<i>Stenella longirostris</i> , <i>Stenella attenuata</i> , <i>Stenella coeruloealba</i> , <i>Stenella frontalis</i> , <i>Stenella clymene</i> , <i>Delphinus delphis</i> , <i>Tursiops truncatus</i> , <i>Sousa plumbea</i> , <i>Steno bredanensis</i> , <i>Lagenorhynchus acutus</i> , <i>Cephalorhynchus heavisidii</i> , <i>Feresa attenuata</i> , <i>Pseudorca crassidens</i> , <i>Globicephala melas</i> , <i>Globicephala macrorhynchus</i> , <i>Phocoena phocoena</i> , <i>Neophocaena phocaenoides</i> , <i>Delphinapterus leucas</i> , <i>Pontoporia blainvillei</i> , <i>Inia geoffrensis</i> , <i>Lioptes vexillifer</i> , <i>Berardius bairdii</i> , <i>Platanista gangetica</i>	$9.3836 \times 10^{-9}$	3.000	0.9574	Perrein et al. 2005
Turtles	<i>Caretta caretta</i> , <i>Chelonia mydas</i> , <i>Eretmochelys imbricata</i> , <i>Dermochelys coriacea</i> , <i>Lepidochelys kempii</i> , <i>Natator depressus</i>	$2.7777 \times 10^{-5}$	2.202	0.9478	<a href="http://www.conserveturtles.org">http://www.conserveturtles.org</a> ; <a href="http://www.dgif.virginia.gov">http://www.dgif.virginia.gov</a>



325

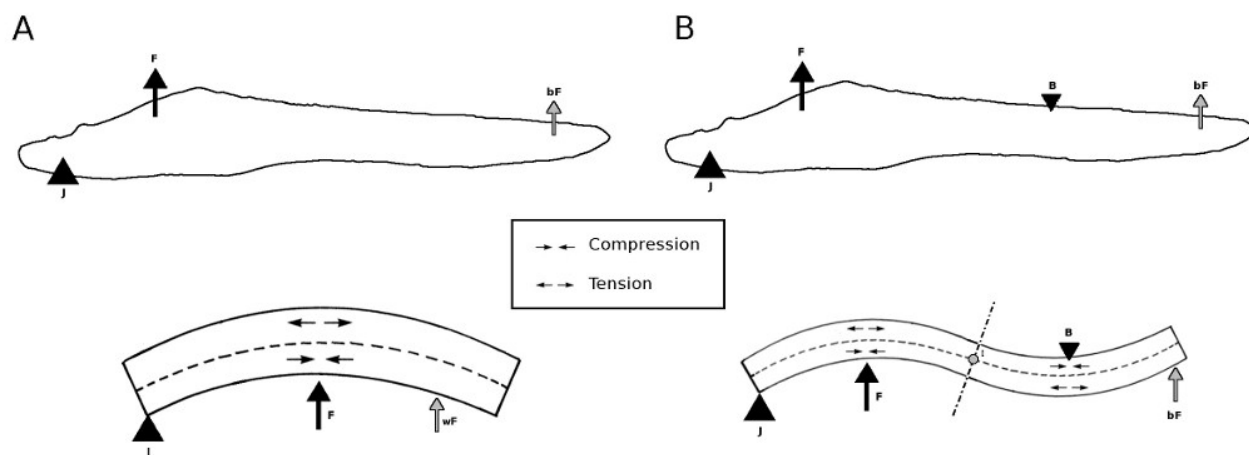


326 **Figure S1.** Schematic reconstruction of DORCM G 13,675 from the digital model. A-B, mandibles,  
 327 dorsal view with bite positions B1-5. C, skull, dorsal view and bite positions S1-3. A, traditional  
 328 unilateral and bilateral lever theory parameters. B, Scheme of caranassial lever (following Greaves  
 329 1983). The scale bar represents 20 cm.



















331 **Figure S2.** FEA model of DORCM G 13,675 working ramus in unilateral loads. A-E, principal  
 332 component strain visualisations S1 (right) and S3 (left). wF, working side force; F, muscle force; J,  
 333 joint constraint at the articular surface; B, bite constraint.

334



335 **Figure S3.** Schematic representation of working and balancing side during unilateral load. A,  
 336 balancing ramus. B, working ramus. Abbreviations: wF, working side force; F, muscle force; J, joint  
 337 constraint at the articular surface; B, bite constraint.

Group	Taxa	Estimated Dimensions			Parameters	
		TL [m]	TW [kg]		L	M
Thalattosuchia	<i>Metriorhynchus cf hastifer</i>	5.42	726		0.480	0.053
	<i>Machimosaurus</i>	up to 9 to 11	up to 3641 to 6893		0.885	0.375
	<i>Metriorhynchus geoffroyii</i>	4.36	363		0.386	0.027
	<i>Metriorhynchus palpebrosus</i>	4.36	363		0.386	0.027
	<i>Dakosaurus maximus</i>	4.5	402		0.398	0.030
	<i>Torvoneustes carpenteri</i>	4.7	461		0.416	0.034
	<i>Gracilineustes acutus</i>	3.8	228		0.333	0.02
	<i>Teleosaurus</i> sp.	3*	119		0.265	0.008
	<i>Steneosaurus</i> sp.	2.5 to 3.5*	61 to 180		0.265	0.008
	<i>Stenosaurus manseli</i>					
	<i>Stenosaurus megarhinus</i>					
	<i>Plesiosuchus manselii</i>	6.8	1493		0.600	0.110
Ichthyosauria	<i>Ophtalmosaurus</i> sp.	6	2026		0.531	0.149
	<i>Aegirosaurus</i>	2	75		0.177	0.01
	<i>Nannopterugius enthekiodon</i>	2.8	206		0.248	0.015
	<i>Brachyptreygius mordax</i>	3	253		0.265	0.02
Pliosauroida	<i>Pliosaurus brachydeirus</i>	-	-		-	-
	<i>Pliosaurus wesburyensis</i>	6.7 to 7.9	2829 to 4638		0.646	0.297
	<i>Pliosaurus 'portentificus'</i>	7.6 to 8.5	4129 to 5777		0.712	0.361
	<i>Pliosaurus carpenteri</i>	7.8 to 9.1	4464 to 7325		0.752	0.430
	<i>Pliosaurus macromerus</i>	11.4 to 12.7	13937 to 19269		1.066	1.212
	<i>Pliosaurus kevani</i>	10.4 to 12.2	10582 to 17082		1.000	1.000
Plesiosauroidea	<i>Plesiosaurus</i> sp.	3.5	220		0.310	0.016
	<i>Colymbosaurus</i> sp.	6	1107		0.531	0.081
	<i>Colymbosaurus trochanterius</i>	6.15	1192		0.544	0.090
	<i>Cimoliasaurus brevior</i>	4 to 7.5	328 to 2161		0.509	0.072
	<i>Kimmerosarus langhami (criptociclidae)</i>	6.6	1473		0.584	0.109
Testudines	<i>Thalassemys hugii</i>	1.2	165		0.106	0.012
	<i>Plesiochelys</i> sp.	-	-		-	-
	<i>Achichelys (Eurysternum)</i> sp.	-	-		-	-
	<i>Peloobatochelys blakei</i>	0.5	24		0.044	0.002
	<i>Pelobatochelys</i> sp.	0.4	14		0.035	0.001
	<i>Tropidemys langi</i>	-	-		-	-

339 Figure S4. Kimmeridgian marine reptile fauna, dimensions and mass. Orange indicates taxa whose

340 dimensions are compatible with seizing; yellow indicates taxa whose dimensions are compatible  
341 with attacks, but for which there is no evidence in pliosaur gut contents. TL, Body Length; TM,  
342 Body Mass;  $RL = BL(\text{taxon})/BL(\text{DORCM G.13,675})$ ;  $RM = BM(\text{taxon})/BM(\text{DORCM G.13,675})$ .  
343 Data are compared with the data available for the largest taxa found in gut content of *Kronosaurus*:  
344  $RL = 0.40$ ;  $RM = 0.034$ ; and  $RL = 0.67$ ;  $RM = 0.161$ , relative to the largest taxon found with bite  
345 marks (McHenry, 2009).



346

347 **Figure S5.** Pliosauridae indet. Undescribed specimen upon which the reconstruction of the  
348 articular-quadrate geometry was based on. Patrick Clarke collection. Scale bar equals 5cm.